



Deposited via The University of Sheffield.

White Rose Research Online URL for this paper:

<https://eprints.whiterose.ac.uk/id/eprint/183471/>

Version: Published Version

Article:

Gan, K.L., Brewer, T.R., Pope, D.J. et al. (2022) Probabilistic analysis of blast-obstacle interaction in a crowded internal environment. *Probabilistic Engineering Mechanics*, 68. 103227. ISSN: 0266-8920

<https://doi.org/10.1016/j.probengmech.2022.103227>

Reuse

This article is distributed under the terms of the Creative Commons Attribution (CC BY) licence. This licence allows you to distribute, remix, tweak, and build upon the work, even commercially, as long as you credit the authors for the original work. More information and the full terms of the licence here:

<https://creativecommons.org/licenses/>

Takedown

If you consider content in White Rose Research Online to be in breach of UK law, please notify us by emailing eprints@whiterose.ac.uk including the URL of the record and the reason for the withdrawal request.



Contents lists available at ScienceDirect

Probabilistic Engineering Mechanics

journal homepage: www.elsevier.com/locate/probengmech

Probabilistic analysis of blast–obstacle interaction in a crowded internal environment

K.L. Gan^a, T.R. Brewer^b, D.J. Pope^c, S.E. Rigby^{a,*}^a Department of Civil & Structural Engineering, University of Sheffield, Mappin Street, Sheffield, S1 3JD, UK^b Synthetik Applied Technologies LLC, 701 Brazos Street, Austin, TX, 78701, USA^c Physical Sciences Group, Platform Services Division, DSTL Porton Down, Salisbury, Wiltshire, SP4 0JQ, UK

ARTICLE INFO

Keywords:

Blast–obstacle interaction
Channelling
Numerical analysis
Monte Carlo
Probabilistic
Shielding

ABSTRACT

Recent terror events such as the Manchester Arena bombing and Brussels and Istanbul airport attacks featured improvised explosive devices detonated in crowded internal spaces. A blast wave that propagates in the presence of obstacles will have fundamentally different properties to those of an unimpeded blast wave. Physical processes such as reflection, diffraction, and superposition of multiple wave fronts result in highly complex and situational-dependent loading characteristics which cannot be predicted using simple tools such as those for predicting free-field blast parameters. The influence of blast–obstacle interaction within an internal environment has not yet been studied. This article uses computational fluid dynamics within a probabilistic framework to quantify the influence of obstacle density and positioning on blast loading characteristics. Two mechanisms which alter the properties of a blast wave are studied: ‘channelling’ and ‘shielding’. It is shown that channelling effects are highly localised and result in increased loading near the explosive, the effect of which increases with obstacle density. Shielding is shown to be a cumulative effect which increases with distance from the explosive, and with increasing obstacle density. Whole-domain cumulative density functions are used to derive quantitative descriptors of the loading characteristics and how they vary relative to simple benchmark cases, with a view to providing clear guidance on the development of future predictive tools.

1. Introduction

Terrorism poses a significant and growing threat to societal safety and stability. Improvised explosive devices (IEDs) are one of the most widely used weapons of terrorists, and accurate and reliable predictions of the blast loading from IED detonations is an ongoing challenge for the protection engineering community. However, prediction of such blast loading is made significantly more complex due to the unpredictable nature of terrorist attacks.

To better characterise the stochastic nature of blast events, previous studies have been carried out to address the intrinsic variability in blast loading caused by uncertainty in parameters such as charge mass, TNT equivalence, stand-off, air temperature, and pressure [1]. In addition to variability introduced by these intrinsic variations, the environment in which the explosive is detonated can significantly alter the properties of the blast wave as it expands and interacts with obstacles [2], termed extrinsic variability. In complex environments, a blast wave will reflect off obstacles, diffract around changes in geometry, and superimpose with other wave fronts in a highly non-linear manner [3]. Recent high-profile terrorist incidents, such as the Manchester Arena bombing (2017, 22 fatalities) and the Brussels Airport attacks

(2016, 33 fatalities), involved the use of high explosives detonated in a crowded internal environment [4,5], and large-scale urban blasts such as the 2020 Beirut explosion [6] produce pressure loadings which differ significantly from the equivalent free-air loading [7].

To account for irregular geometry-induced shock wave interactions, computational fluid dynamics (CFD) has been successfully used to simulate the resultant blast loading in public spaces [8–10] and cityscapes [11–14]. However, the distribution of obstacles in an indoor environment may be complex and varying with time, meaning numerical results based on a single deterministic model may not be representative of the entire range of possible outcomes [8,15]. Therefore, a probabilistic approach should be undertaken in order to truly understand the influence of obstacles on blast loading in a crowded internal environment.

This paper investigates the interaction of blast waves with randomly positioned obstacles within a crowded internal environment using computational fluid dynamics. Obstacle positions are varied randomly according to a series of pre-determined densities and biases, with each configuration repeated a large number of times using the Monte Carlo method (e.g., a given obstacle density and bias but with random obstacle placement in each) to develop statistically robust datasets.

* Corresponding author.

E-mail address: sam.rigby@shef.ac.uk (S.E. Rigby).

<https://doi.org/10.1016/j.probengmech.2022.103227>

Received 29 September 2021; Received in revised form 5 January 2022; Accepted 2 February 2022

Available online 9 February 2022

0266-8920/© 2022 Elsevier Ltd. All rights reserved.

Cumulative density functions and median values were determined for the entire domain to enable general observations to be drawn on the magnitude and range of loading in each case. Finally, blast parameters are compiled against scaled distance from the blast, and compared against the empty room case, to enable conclusions to be drawn on the effects of obstacle distribution and density, and the prominence of channelling and shielding effects with respect to distance from the explosive. The overall aim of this study is to provide guidance on how to modify simple loading (e.g., in an empty room) to account for the presence of obstacles within the domain.

2. Literature review

2.1. Blast–obstacle interaction

Shock tube testing has been utilised extensively to study the interaction between blast waves and rigid obstacles. When a blast wave passes through an array of cylindrical obstacles, both an increase in pressure upstream of the obstacles (due to reflection) and a decrease in pressure downstream of the obstacles (due to attenuation) has been observed [16]. Reducing the net flow area of the array through inclusion of a higher number of obstacles or obstacle layers results in better attenuation [17]. Additionally, Suzuki et al. [16] and Chaudhuri et al. [18] noted small differences in attenuation between a staggered and regular obstacle array arrangement, with the staggered arrangement achieving slightly better attenuation. The influence of obstacle shape was also studied, with Chaudhuri et al. [18], Wan & Eliasson [19] and Prasanna Kumar et al. [17] finding that an array of reverse triangular prisms or squares achieve higher attenuation than cylindrical arrays. Hahn et al. [20] studied blast interaction with a single cylindrical column and found that the presence of a semi-infinite wall closely behind the column would substantially increase blast overpressure.

When considering blast–obstacle interaction in a crowded environment, the potential effect of Mach reflection from the ceilings and diffraction effects across the top of obstacles cannot be ignored [21]. Hajek & Folgar [22] and Gautier et al. [23] found some evidence to suggest that the attenuation effect of finite-height obstacle arrays on blast overpressure was either negligible or even disadvantageous. This is thought to be caused by the diffraction of blast waves above the obstacles [23], which was not present in previous studies due to the 2D nature of those problems. In contrast to the findings in [22,23], Xiao et al. [24,25] found a correlation between downstream impulse attenuation and number of square posts, in a single-layered barrier, and the results were generally consistent regardless of obstacle height.

Downstream impulse enhancement observed in the previous studies can be explained by the transmitted and diffracted waves superimposing directly behind the obstacle. Whilst these studies are, by design, comparable to equivalent free-field explosions, no research has yet considered blast–obstacle interaction within an internal environment. It is hypothesised that transmitted-diffracted wave superposition in particular will be made significantly more complex due to additional confinement and the larger number of reflecting surfaces present. Furthermore, since most studies on obstacle arrays are done so with the intention of designing novel blast barriers, the arrangements of obstacles studied thus far have been systematic and predetermined.

In the context of explosions in cityscapes, Smith et al. [26] varied the confinement provided by different street junctions and found that stronger confinement produces higher specific impulse values along the street due to blast wave channelling. It has also been shown that street width and building height affects the location and intensity of this amplification [27]. Experimental studies on blast propagation through semi-detached housing blocks showed that the average transmitted impulse increased with increasing areal density of the buildings [28]. As both channelling (enhancement) and shielding effects (mitigation) were observed, it was suggested that channelling effects are generally dominant owing to the increase in transmitted impulse with aerial

density. In order to assess possible variations in street configurations, Smith et al. [28] randomised the position of housing blocks but found small differences between regular and random rectangular obstacle arrangement, albeit within the limited parameter space tested. It was tentatively suggested that impulse enhancement was a function of areal density alone, and invariant of whether there was a clear or obstructed propagation path for the blast wave.

There have also been numerous efforts to investigate detonation events in a confined public setting such as train stations, train carriages, tunnels, indoor lobbies, and metro lines using numerical methods [8,9,22,29,30]. However, these studies are focused on the confining geometry of the spaces, and the presence of obstacles within the domain has not yet been studied.

2.2. Probabilistic blast analysis

The Monte Carlo method is commonly used in the literature to incorporate the uncertainty of urban explosions in numerical analysis [31]. This involves randomly generating inputs according to a given statistical distribution and solving a large number of configurations in order to assess how the uncertainty associated with the input parameter propagates through to the output.

Seisson et al. [31] implemented normal distribution to the uncertainties in material and geometric properties of masonry panels, showing its applicability in estimating the failure probability and required security perimeter using the single-degree-of-freedom method. Shi & Stewart [32] incorporated spatial variation in the material properties and blast loading in their Monte Carlo assessment of reinforced concrete columns. Introducing uncertainties to the model errors as well as charge and material properties, Netherton & Stewart [33] detailed the probability of glazing safety hazards at various scaled distances. To estimate the probability of progressive collapse for steel frame structures under blast loading, Ding et al. [34,35] further utilised a more sophisticated Markov Chain Monte Carlo simulation algorithm to improve upon the accuracy and efficiency of conventional Monte Carlo methods.

Alterman et al. [9] conducted a probabilistic analysis of blast inside a typical ground floor lobby (without the presence of obstacles), to better quantify fatality risks due to IED explosions. This framework was extended by Marks et al. [36] to study fatality risks due to the pressure and impulse from a vehicle-borne IED detonated at a T-junction in an urban streetscape.

In summary, the Monte Carlo method is a robust tool to provide statistical descriptions of intrinsic and extrinsic blast parameter variability to inform risk-based analysis and design. It is known that the presence of obstacles can provide either enhancement or mitigation of blast pressures through a combination of channelling and shielding effects. Key parameters known to influence blast properties are: the density of obstacles; obstacle geometry; and arrangement of obstacles. Blast–obstacle interaction in a crowded building space has not yet been studied, and the overall effects of obstacle positioning are not known.

3. Numerical modelling

3.1. *blastFoam*

blastFoam (version 4.0) is an open-source CFD solver for simulating blast events [37] and is used for the computational analyses in this study. The Navier–Stokes equations form the basis for the simulation of highly compressible fluid in *blastFoam*, as shown below:

$$\partial_t \mathbf{U} + \nabla \cdot \mathbf{F} = \mathbf{S} \quad (1)$$

where \mathbf{U} is the vector of conservative variables, volume fraction, mass, momentum, and energy, \mathbf{F} are the fluxes corresponding to the respective conservative variables, and \mathbf{S} is a vector of source terms [37]. Three components – an equation of state, a thermodynamic model and

Table 1
blastFoam models used for C4 and air.

	C4		Air
	Reactants	Products	
Equation of state	Murnaghan	Jones Wilkins Lee (JWL)	Ideal gas
Thermodynamic model	eConst	eConst	eConst
Transport model	Const	Const	Const

a transport model – are used to calculate temperature and pressure of the fluid given the conservative quantities.

Internal energy is calculated from the thermodynamic model based solely on thermal contribution. Though both internal energy and temperature-based equations of state are available in *blastFoam*, the former is chosen for this study. This allows for pressure to be calculated using the Mie-Gruneisen form.

Transport models define quantities such as viscosity and thermal diffusion. To describe a detonating material, a model that transitions from an unreacted state (reactants) to reacted state (products) through an activation model is implemented in *blastFoam*. Both states are specified by their own components (equation of state, thermodynamic and transport model). Different activation models are used to describe the speed at which solid reactants are converted to gaseous products. To initialise the internal energy, pressure and density are used. A Newton–Raphson root finding method is then used to solve for the necessary quantities. Overall, the models used for all three components are shown in Table 1.

Note that *eConst* represents constant specific heat at constant volume and *Const* represents constant values for viscosity and Prandtl number. For this study, the linear activation model is used, where a constant detonation velocity is used to identify activated cells from a user-specified point of initiation. As an explicit solver, *blastFoam* is set to utilise the Tadmor flux scheme. Time integration is achieved using second-order, strong stability-preserving Runge–Kutta method (RK2SSP). Further detailed theory of the *blastFoam* solver can be found in the *blastFoam* User Guide [37].

Output from *blastFoam* compares well against the Kingery–Bulmash semi-empirical formulations [38] and numerous other CFD codes commonly used within the industry such as Autodyn, LS-Dyna, CTH and EPX [39]. *blastFoam* has also been extensively validated against 2D and 3D data currently available in the literature [40], e.g., the 2D Riemann problem [41], double Mach reflection [42], 2D and 3D Sedov problems [43], and experimental test data across a range of scales and scaled distances [44–47]. A number of validation examples are provided in the *blastFoam* GitHub repository [48]. Hence, *blastFoam* can be used with confidence to study blast–obstacle interactions in this article.

3.2. Model set up

3.2.1. Model domain and explosive representation

In this study, a domain size of a 15×15 m on plan was chosen to be representative of a typical internal environment [9,10]. The side edges of the domain were specified as outflow boundaries, on the assumption that pressures and impulses at the domain edges will be several orders of magnitude lower than those close to the explosive.¹ This also facilitates future studies on room size and provides a representative benchmark. The ceiling was located 6 m above ground level (set as a rigid reflecting surface), and a typical suitcase bomb of 23 kg TNT equivalent was placed at the centre of the domain, 1 m above ground level, as per the study by Alterman et al. [9]. Blast–obstacle interaction effects have been shown to be more significant for strong

¹ The influence of rigid walls was investigated in Ref. [49], however it was found that blast profiles were only affected at points most remote from the charge.

shock conditions [50] and longer blast durations [51], justifying the choice of a relatively large charge mass.

The explosives were modelled as C4, using the default material and equation of state parameters provided for C4 in *blastFoam*. A TNT equivalence of 1.2 was used [52], where TNT equivalence is defined as the equivalent mass of TNT required to produce a blast wave of equal magnitude to that produced by a unit weight of the explosive in question [53]. Therefore, a 19.17 kg charge mass was required to achieve a 23 kg TNT equivalence. A radius of 0.142 m was specified, given a density of 1601 kg/m^3 . All analyses were terminated after 25 ms, to allow sufficient time for the blast wave to propagate through the domain and interact with the obstacles. The cell size of the domain was set to be 0.5 m, with an Adaptive Mesh Refinement (AMR) level of 2. This results in a minimum cell size of 125 mm, and is comparable to the 100 mm element size used in Ref. [9]. The typical analysis time was 200 minutes, which was deemed necessary to enable a large number of simulations to be run in a reasonable time.

AMR is a method of adapting the mesh resolution (i.e., cell edge length) of a computational domain within certain regions of interest (e.g., the shock front), dynamically during the simulation; increasing the precision in specific areas while leaving other regions of the domain at lower levels of resolution. AMR in *blastFoam* is based on the work of Rettenmaier et al. [54], and operates for 2D, 2D axi-symmetric, and 3D computational domains. Furthermore, user-specified ‘probe’ locations are automatically refined up to the maximum level of refinement specified within the domain to avoid discontinuities in probe sampling.

blastFoam also incorporates dynamic load balancing to mitigate potential memory issues such as crashing and slow-down related to overloading CPUs that are operating on zones of high refinement. At a predetermined user-defined timestep interval the computational domain is ‘rebalanced’ so that the cell count per CPU is more evenly distributed. This concept is illustrated in Fig. 1.

3.2.2. Obstacle representation

Sielicki & Gajewski [55] numerically studied the response of human torsos to near-field blast loads, and found that at a scaled distance of $1 \text{ m/kg}^{1/3}$, maximum displacements of the head and torso were <2 mm. This suggests that modelling human obstacles as representative rigid obstacles is a reasonable simplification as the displacement is expected to be negligible during loading. Whilst a small number of obstacles may be placed at scaled distances $<1 \text{ m/kg}^{1/3}$ in the current work (the minimum scaled distance from the charge to an obstacle is set at $0.25 \text{ m/kg}^{1/3}$), the effects of obstacle compliance on the representative loading in the entire domain is still expected to be minimal.

In order to further reduce complexity (in particular of the mesh, and the algorithms required to detect overlap when placing new obstacles in the domain), the obstacles were modelled as cylinders, after Pope [56]. This also removes the need to account for random obstacle orientation. The width of the cylindrical obstacle is derived from the Hybrid III dummy, as per the study by Sielicki & Gajewski [55]. This results in a shoulder width of 0.4 m, rounded from 0.429 m [57]. The height of the obstacle is set to be 1.7 m, as a simplified average of the population height in the UK [58].

The cylindrical obstacles for each of the simulation runs were generated as a single Standard Tessellation Language (STL) geometry file by a bespoke obstacle generation and placement script written in MatLab. The STL files imported into the computational domain (i.e., the encompassing volume of air within the room, created by the *blockMesh* utility) at run-time by the *snappyHexMesh* utility. Once meshed, each of the cylinders created a sub-volume and the user specified ‘locationInMesh’ point directs *snappyHexMesh* to retain the volume of interest (i.e., the surrounding air in the room) whilst subtracting all the cylindrical obstacle sub-volumes.

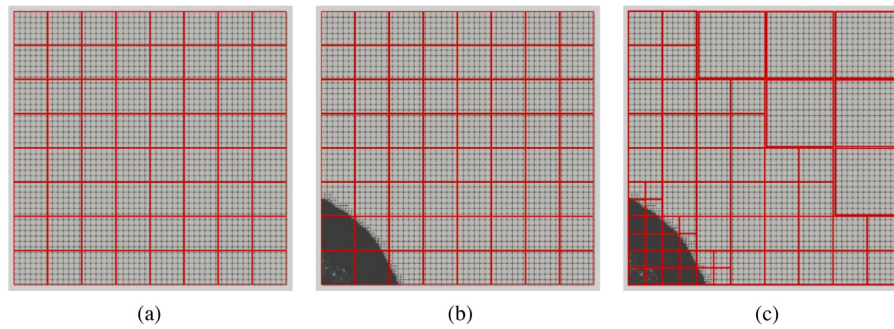


Fig. 1. AMR and dynamic load rebalancing in *blastFoam*. (a) initial domain subdivision with 64 CPUs [denoted by the red boxes], (b) AMR acting in areas of high pressure resulting in load imbalance, and (c) computational burden balanced more evenly across the 64 CPUs. Source: Adapted from [39].

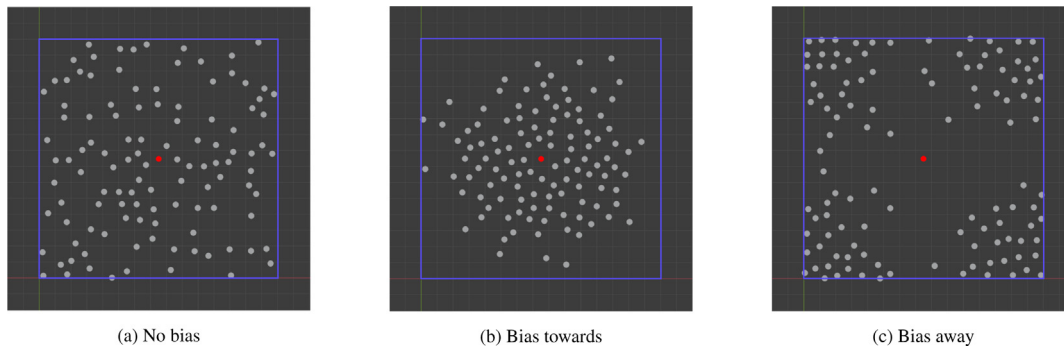


Fig. 2. Example obstacle arrangements for the (a) no bias, (b) bias towards, and (c) bias away cases.

3.2.3. Data collection

For each simulation, an array of pressure probes were placed throughout the numerical domain as a 16×16 grid at 1 m intervals, along the plane of the centre of the charge (1 m above ground level, after Ref. [9]), resulting in 256 measurement locations per run. If a probe was found to overlap with an obstacle, the probe was automatically repositioned to the nearest free node in the mesh, and its new position recorded and used thereafter, e.g., when compiling results with distance.

3.3. Probabilistic framework

3.3.1. Obstacle arrangements

In order to account for variations in obstacle arrangement in a crowded internal space, three types of distribution were modelled. These are termed ‘no bias’, ‘bias towards’, and ‘bias away’, as per Fig. 2.

- **‘No bias’, Fig. 2(a):**
Obstacles were positioned randomly in the domain, in-turn, using a purpose-written MatLab script. Random x and y coordinates were generated from a uniform distribution from 0–15 m, and provided the obstacle did not overlap a previously-placed obstacle or the charge (see below), it was placed in the domain and the next random coordinates were generated. This process was repeated until the domain had been filled to the specified obstacle density. For the ‘no bias’ arrangement, four obstacle densities were specified: 0.2, 0.5, 1.0, and 1.4 obstacles/m². These correspond to ‘Levels of Service’ B, D, E, and F for walkways and sidewalks, as given by the United States of America Transportation Research Board and summarised in Daamen [59].
- **‘Bias towards’, Fig. 2(b):**
Obstacles were positioned according to a normal distribution, with a mean of 7.5 m in both x and y . Two different standard deviations were modelled: 2.29 m and 3.40 m. These represent probabilities of 90% and 75% of an obstacle being placed within

3.75 m of the charge, respectively [49]. Obstacles were placed at a density of 0.5 obstacles/m² only.

- **‘Bias away’, Fig. 2(c):**

Obstacles were placed as above, but with the normal distributions inverted such that standard deviations of 2.29 m and 3.40 m relate to 90% and 75% probability of an obstacle being placed *further* than 3.75 m from the charge. Obstacles were placed at a density of 0.5 obstacles/m² only.

The minimum spacing between obstacles was set to 0.7 m (between centres) in order to retain a regular mesh at AMR level 2. The minimum spacing between the explosive centre and the nearest obstacle was also set to 0.7 m for the same reason.

3.3.2. Parametric study overview

The parametric study consists of eight different obstacle configurations (‘cases’), plus a benchmark case with no obstacles present (termed ‘Empty room’). Twenty simulations (‘runs’) were performed for each of the cases with obstacles, resulting in 161 total simulations and approximately 540 h of total simulation time. The naming convention used in this article is summarised in Table 2. Hereafter, ‘D0.5’ is referred to as the ‘datum’ case when assessing the influence of obstacle density and positioning bias.

3.4. Example output

3.4.1. Example ‘bias away’ run

Fig. 3 shows example output from a ‘bias away’ run. Here, fringe plots of peak specific impulse are shown for 1.00, 2.50, 5.00, and 7.50 ms after detonation (only impulse values acting on rigid surfaces are shown for clarity of presentation). It can be seen that whilst the blast wave is perfectly hemispherical in the early stages, it rapidly degrades once it begins interacting with the rigid obstacles. Complex wave fronts are visible at 7.50 ms after detonation, and there is evidence of shielding behind the obstacles nearest the charge, particularly visible in the 5.00 ms plot.

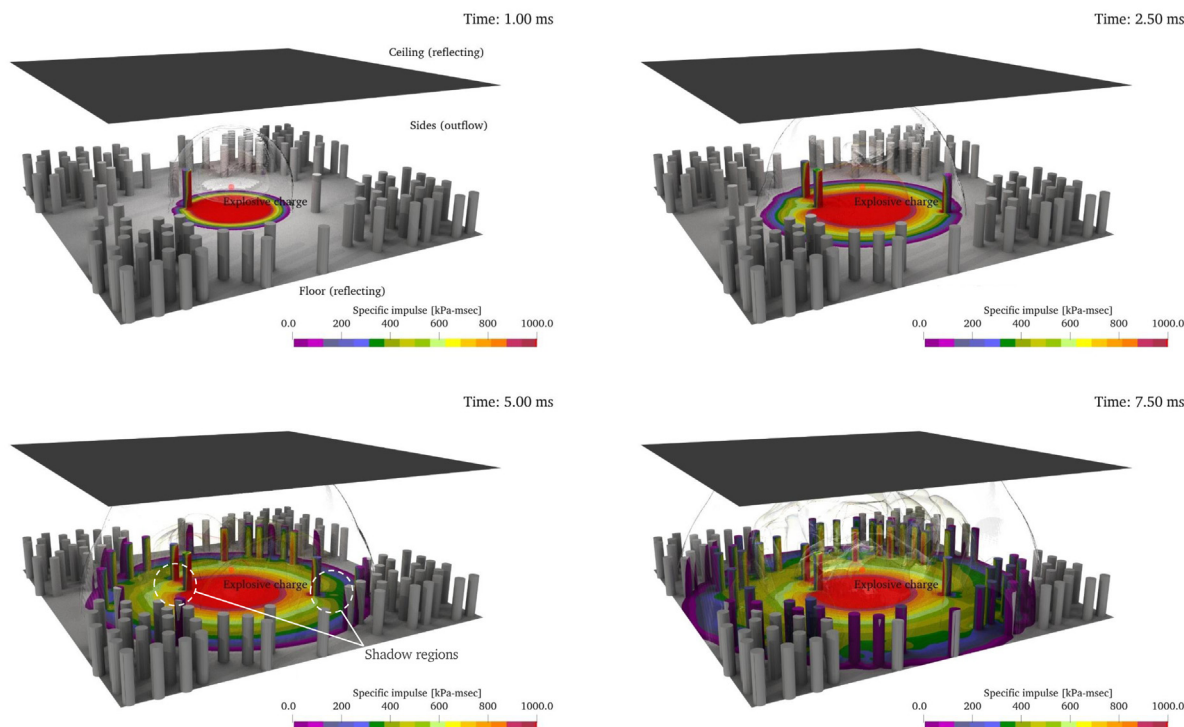


Fig. 3. Example output from a ‘bias away’ run, with prominent shadow regions at $t = 5.00$ ms highlighted.

Table 2
Naming convention and details of each case tested in the parametric study.

Case	Obstacle density (obstacles/m ²)	Positioning bias	Runs
Empty room	0	No bias	1
D0.2	0.2	No bias	20
D0.5	0.5	No bias	20
D1.0	1.0	No bias	20
D1.4	1.4	No bias	20
BT2.29	0.5	Bias towards ($\sigma = 2.29$ m)	20
BT3.40	0.5	Bias towards ($\sigma = 3.40$ m)	20
BA2.29	0.5	Bias away ($\sigma = 2.29$ m)	20
BA3.40	0.5	Bias away ($\sigma = 3.40$ m)	20

3.4.2. Compiled specific impulse

Overpressure histories were recorded at each probe for the duration of the simulation (25 ms), and specific impulse was determined through numerical integration of the pressure histories with respect to time. For each probe, peak values of pressure and specific impulse are of interest, with peak pressure taken as the maximum pressure recorded by the probe, and peak specific impulse taken as the maximum specific impulse recorded within 10 ms of arrival of the blast² at the probe location. A cut-off of 10 ms was selected to negate the effect of expansion waves from the boundaries corrupting the signal and affecting the pressure readings, and a consistent approach was taken throughout to ensure validity of test-to-test and case-to-case comparisons.

Thus, there are 256 pairs of peak pressure and peak specific impulse per run, and 256×20 pairs per case. Due to the random placement of the obstacles, each set of 256 pressure/impulse pairs will differ somewhat. This effect is illustrated in Fig. 4, which shows example peak specific impulse distributions within the domain for three different runs in the ‘no bias’ (0.5 obstacles/m²), ‘bias towards’ (0.5 obstacles/m², $\sigma = 2.29$ m), and ‘bias away’ (0.5 obstacles/m², $\sigma = 2.29$ m) cases.

² Arrival time is defined in this study as the time at which the probe signal exceeded 10 Pa above ambient pressure

The channelling and shielding effect of the obstacles can be clearly seen. The distributions are highly irregular, with localised areas of high magnitude – e.g., (8, 5) in Fig. 4(c), and (9, 8) in Fig. 4(g) – indicating areas where the blast has reflected off an obstacle and/or been channelled by neighbouring obstacles. Further, shadow regions – e.g., (9, 12) in Fig. 4(a), and (14, 6) in Fig. 4(f) – indicate areas where probes are situated immediately behind an obstacle and have benefited from the shielding effect. Whilst the specific impulse distributions and hence channelling/shielding effects differ on a run-by-run basis, there appear to be some consistencies when viewing the cases as a whole. Compared to the ‘no bias’ case, a bias towards the charge increases the specific impulse experienced in the domain centre whilst subsequently reducing the specific impulse at the periphery of the domain. Conversely, a bias away from the charge appears to reduce the magnitude of the central specific impulse, with this intermediate specific impulse acting across a much larger area of the domain, extending into regions where the ‘no bias’ and ‘bias towards’ cases exhibit relatively lower impulses. These example results indicate that obstacle arrangement may have significant influence on the loading experienced within the domain.

4. Results and discussion

4.1. Whole domain results

4.1.1. Generation of cumulative distribution curves

For each case, all 5,120 pairs of peak pressure and peak specific impulse were compiled into cumulative distribution curves. These indicate the probability that the pressure/impulse at a randomly-picked point in the domain will not exceed a certain value, and therefore can be used to draw conclusions on the representative loading within the domain. Two types of statistical measure are used to make quantitative comments on the cumulative distributions: 5th, 50th (median), and 95th percentiles, and standard deviation. The standard deviation is analogous to the slope of the curve.

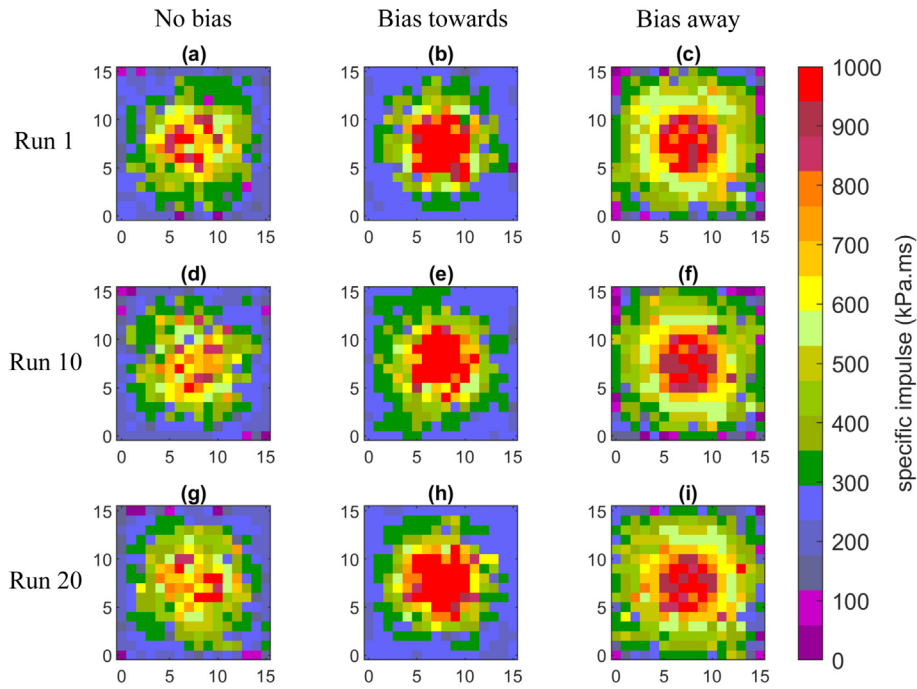


Fig. 4. Fringe plots of peak specific impulse for different parametric variations of no bias (a, d, g), bias towards (b, e, h), and bias away (c, f, i). Results from the 1st (a, b, c), 10th (d, e, f), and 20th (g, h, i) runs for each case are shown.

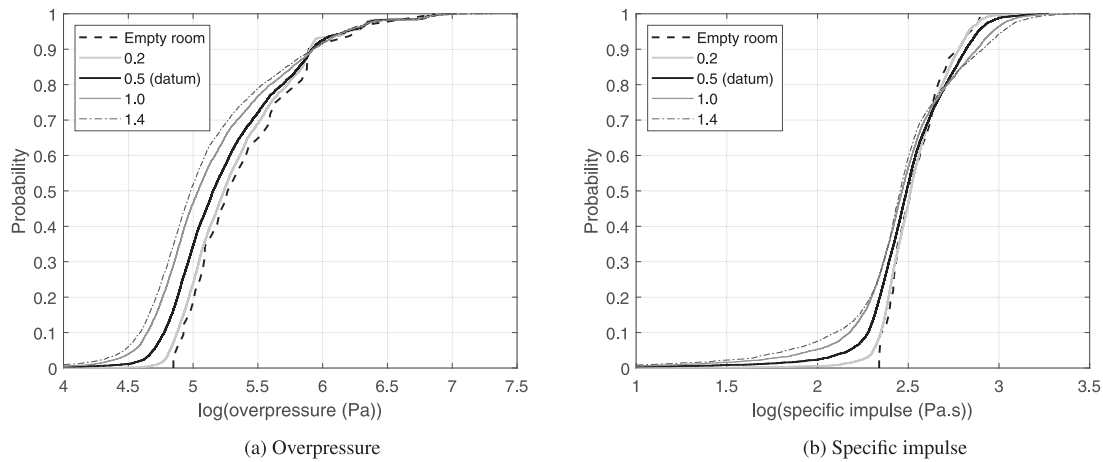


Fig. 5. Overpressure (a), and specific impulse (b) cumulative distribution curves for obstacle densities of 0.0, 0.2, 0.5, 1.0, and 1.4 obstacles/m².

4.1.2. Effect of obstacle density

Fig. 5 shows the effect of obstacle density on peak overpressure (a) and peak specific impulse (b). With reference to the overpressure curves, it can be seen that the presence of obstacles leads to a general shift to the left, with the higher obstacle densities leading to a more substantial shift and therefore a more significant reduction in peak pressure throughout the domain. Interestingly, the curves converge at a probability of approximately 0.85, suggesting that the largest pressures in the domain (i.e., those closest to the charge) remain unaffected by the presence or density of obstacles.

The influence of obstacle density on specific impulse is similar, albeit less pronounced, with the curves appearing to flatten as obstacle density increases. This suggests that the variability of loading increases with increasing obstacle density. Comparing the 1.4 obstacles/m² curve with the empty room curve: there is a 20% probability that the specific impulse will be below 10^{2.3} Pa.s in the former, and a 0% probability in the latter. Conversely, there is a 10% probability that the specific impulse will exceed 10^{2.7} Pa.s in the 1.4 obstacles/m² case, and a 0%

probability that the impulse will exceed this value in the empty room case.

Since higher magnitude blast parameters are located closer to the charge, and lower magnitude blast parameters are located further away, the results indicate that the channelling effect is dominant closer to the charge (higher values increase with increasing density), and that the shielding effect becomes progressively important as distance from the charge increases (lower values decrease with increasing density). This suggests that the shielding effect is somewhat cumulative. As the blast propagates outwards from the centre of the domain, it initially encounters few obstacles, and a number of preferential pathways are established. As the blast wave continues to propagate, it encounters more obstacles and the pathways begin to close. As distance from the blast increases, the likelihood that a preferential pathway (channelling) will be obstructed (thereby reverting to shielding) increases.

As shown in Table 3, an increase in obstacle density results in a decrease in the 5th and 50th percentile values of both peak overpressure and peak specific impulse. The pressure 95th percentiles remain

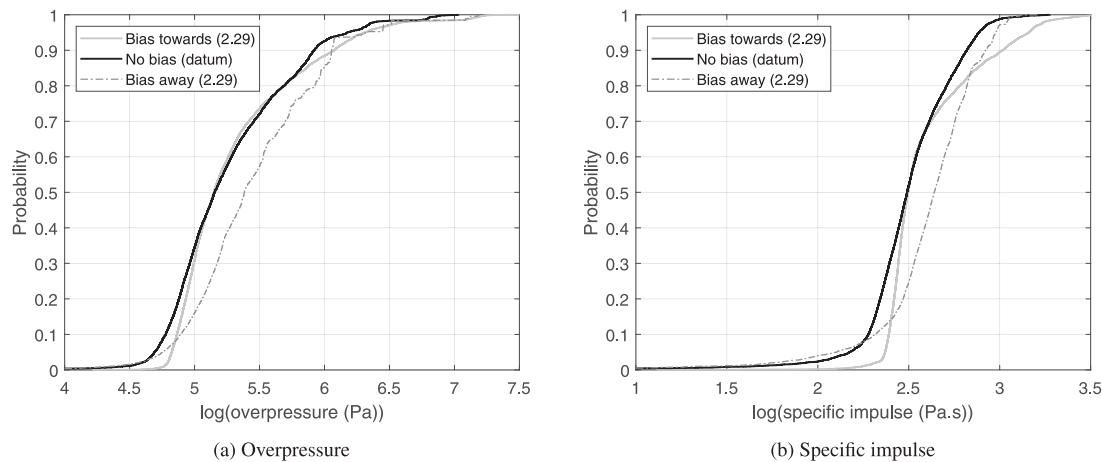


Fig. 6. Overpressure (a), and specific impulse (b) cumulative distribution curves for ‘no bias’, ‘bias towards’ ($\sigma = 2.29$) and ‘bias away’ ($\sigma = 2.29$) cases.

Table 3

5th, 50th, and 95th percentiles, and standard deviations for whole domain overpressure and specific impulse as a function of obstacle density.

Obstacle density (obstacles/m ²)	Overpressure (kPa)				Specific impulse (kPa s)			
	Percentile			σ	Percentile			σ
	5th	50th	95th		5th	50th	95th	
0.0	84	191	1619	0.880	222	327	653	0.141
0.2	66	173	1573	0.903	203	325	682	0.164
0.5	49	143	1496	0.935	150	309	768	0.209
1.0	35	109	1488	0.969	96	289	925	0.266
1.4	29	96	1458	1.030	68	281	1045	0.318

relatively unchanged, whereas the 95th percentile specific impulses increase with increasing obstacle density, as noted previously. This is accompanied by an increase in standard deviation with respect to obstacle density, in both cases.

The median pressure at 1.4 obstacles/m² is approximately half the median pressure in the empty room, whereas the median impulse at 1.4 obstacles/m² is approximately 86% of the median impulse in the empty room. Conversely, the pressure standard deviation at 1.4 obstacles/m² is approximately 17% greater than the empty room case, whereas the impulse standard deviation at 1.4 obstacles/m² is more than double the empty room case. This shows that the presence of obstacles has the most pronounced effect on decreasing the magnitude of pressure (compared to impulse) and increasing the variability of impulse (compared to pressure).

4.1.3. Effect of obstacle bias

The effect of obstacle bias on the whole domain loading parameters is shown in Fig. 6. Here, it can be seen that a bias towards the charge slightly increases the prevalence of higher pressures and impulses, as is to be expected given that a larger number of obstacles are located closer to the explosive, resulting in enhanced reflections and channelling.

The higher concentration of obstacles close to the charge slightly reduces the prevalence of lower pressures and impulses, which is likely due to the fact that the shielding effect at larger distances is lessened due to the bias resulting in relatively lower number of obstacles placed further from the charge. The effect of shifting the bias away from the charge is seen as a general increase in the peak pressures and impulses within the domain, and is indicative of a lessening of the shielding effect. Again, this is to be expected due to the cumulative nature of the shielding effect: fewer obstacles between the probe and the explosive lessens the effect. This matches the qualitative observations in Section 3.4, i.e., reduced magnitude central impulses with

Table 4

5th, 50th, and 95th percentiles, and standard deviation values for whole domain overpressure and specific impulse as a function of obstacle bias.

Obstacle bias	Overpressure (kPa)				Specific impulse (kPa s)			
	Percentile			σ	Percentile			σ
	5th	50th	95th		5th	50th	95th	
No bias	49	143	1496	0.935	127	309	768	0.209
BT2.29	67	141	2049	1.979	235	314	1447	0.431
BT3.40	48	125	1527	1.067	180	287	907	0.260
BA2.29	56	242	2138	1.714	126	436	952	0.242
BA3.40	63	223	2121	1.704	157	413	1013	0.263

intermediate-level impulses acting over a larger area relative to the ‘no bias’ case.

Fig. 7 shows the effect of degree of bias on the whole domain results. The cumulative probability distributions are highly similar for both ‘bias away’ cases, with slight variations in the ‘bias towards’ cases. Here, decreasing the degree of bias (i.e., increasing the standard deviation) brings the results more in-line with those from the ‘no bias’ case, as is to be expected. It can be concluded, therefore, that degree of bias has a second-order influence.

5th, 50th, and 95th percentiles, and standard deviations for the obstacle bias cases are compiled in Table 4. It can be seen that decreasing the degree of bias leads to a modest decrease in the median overpressure and specific impulse. Decreasing the degree of balance results in a clear reduction in standard deviation for the ‘bias towards’ cases, although the influence of degree of bias on standard deviation for the ‘bias away’ cases is inconclusive. A larger standard deviation is indicative of a shift from channelling to shielding. This explains why the standard deviations for the BT2.29 case are considerably higher than all other cases: whilst the blast is initially channelled by the obstacles closest to the charge, there is a higher proportion of obstacles immediately behind these, and therefore the likelihood that a preferential pathway is closed and the mechanism reverts to shielding, which is increased.

4.2. Relationship with scaled distance

4.2.1. Generation of scaled distance curves

To quantify the effects of obstacles as a function of scaled distance, all 5,120 pairs of peak pressure and peak specific impulse were grouped by scaled distance, in increments of 0.4 m/kg^{1/3}, and are plotted in the range 0.4–3.6 m/kg^{1/3}. Scaled distance is defined as the distance from the explosive centre divided by the cube-root of the charge mass, according to Hopkinson–Cranz scaling [60]. In each scaled distance interval, the median pressure and impulse are evaluated.

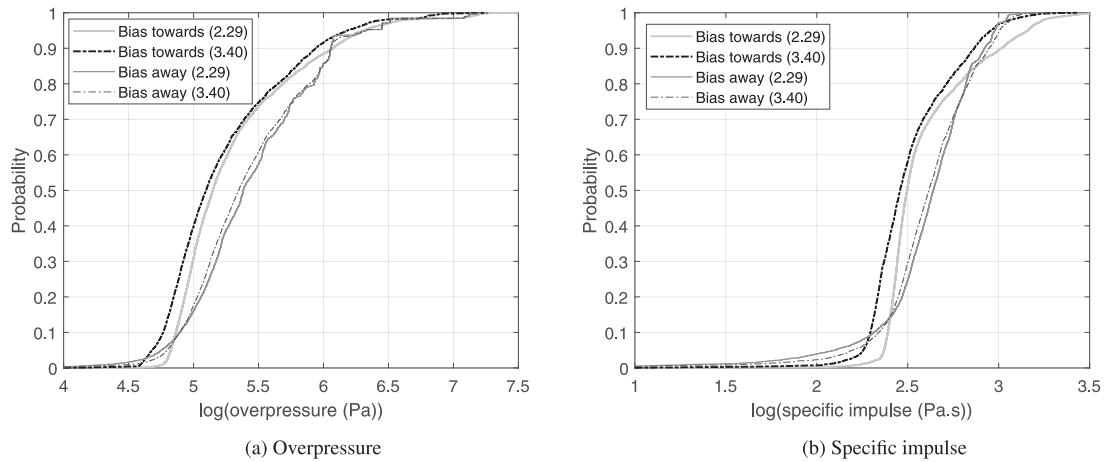


Fig. 7. Overpressure (a), and specific impulse (b) cumulative distribution curves for ‘bias towards’ and ‘bias away’ cases with different standard deviations.

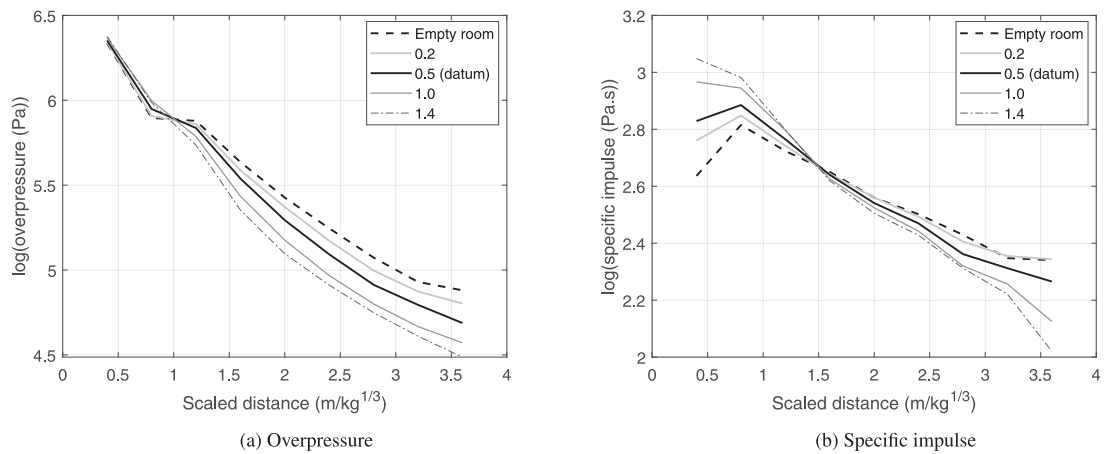


Fig. 8. (a) Overpressure and (b) specific impulse versus scaled distance for obstacle densities of 0.0, 0.2, 0.5, 1.0, and 1.4 obstacles/m².

4.2.2. Effect of obstacle density

Fig. 8 shows the relationship between scaled distance, obstacle density, and peak pressure and peak specific impulse. Values of pressure and impulse greater than the empty room case suggest that channelling effects are dominant, and values lower than the empty room case suggest that shielding effects are dominant.

As noted previously, the pressure curves show little differences close to the charge, whereas the impulse curves show evidence of impulse trapping and enhancement. At the nearest scaled distance, the peak specific impulse in the 1.4 obstacles/m² case is 2–3 times higher than the peak specific impulse at the same scaled distance in the empty room. As scaled distance increases, the effects of shielding begin to dominate, and the curves show progressively increasing reductions in both pressure and impulse with increasing obstacle density. Interestingly, the impulse curves are all approximately equal at a scaled distance of 1.5 m/kg^{1/3}, signifying the point where the enhancement caused by channelling and the attenuation caused by shielding cancels out. At the furthest scaled distance, the peak pressure and peak specific impulse in the 1.4 obstacles/m² case are around half those at the same scaled distance in the empty room.

4.2.3. Effect of obstacle bias

Fig. 9 shows the relationship between scaled distance, obstacle bias, and peak pressure and peak specific impulse. Due to the second-order nature of the degree of bias, BA3.40 and BT3.40 are omitted.

The ‘bias away’ case exhibits a greater peak pressure and specific impulse than both the empty room and ‘no bias’ cases for all but the largest scaled distance. As discussed previously, this is due to

the lessened opportunity of shielding at small and intermediate scaled distances owing to a higher proportion of obstacles being placed further from the charge. Noticeable decreases in pressure and impulse occur at approximately 3.0 m/kg^{1/3}, due to the blast wave encountering a larger number of obstacles and hence shielding increasing, relative to all other cases.

The ‘bias towards’ case exhibits considerably larger pressure and impulses closer to the charge owing to trapping and channelling, although these values become comparable to the ‘no bias’ cases at intermediate scaled distances (1.5–2.5 m/kg^{1/3}). Pressure and impulse are seen to increase slightly relative to the ‘no bias’ case at larger scaled distances due to the relatively fewer number of obstacles and hence reduced opportunity for shielding, in opposition to the reduction seen in the ‘bias away’ case.

5. Summary and conclusions

Probabilistic analysis provides a framework for studying the effects of both intrinsic (relating to uncertainties in input parameters such as charge composition, placement, and ambient conditions) and extrinsic (relating to the setting in which the explosive is detonated, e.g., a cityscape or crowded internal environment). Blast–obstacle interaction is known to introduce two mechanisms which alter the properties of a blast wave: ‘channelling’ and ‘shielding’. The former, caused by the provision of preferential pathways for the blast wave to propagate through, leads to an overall increase in loading parameters due to trapping and confinement effects. The latter, caused by obstacles obstructing

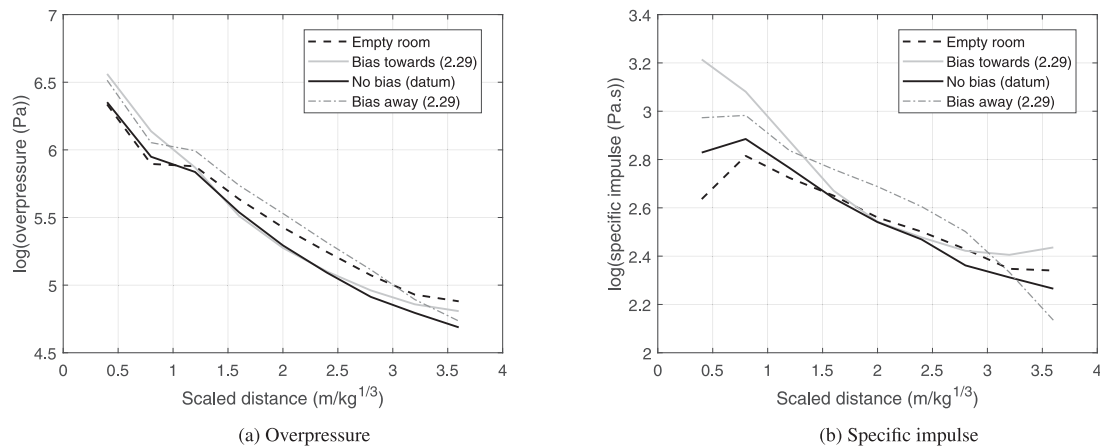


Fig. 9. (a) Overpressure and (b) specific impulse versus scaled distance for different obstacle bias.

and diverting the blast wave, leads to an overall decrease in loading parameters.

The computational fluid dynamics solver *blastFoam* has been used to simulate a large number of explosions within a crowded environment. Specifically, a large number of obstacles (1.7 m height, 0.4 m diameter rigid cylinders) were randomly-placed within a $15 \times 15 \times 6$ m domain, representing a typical internal space. The explosives were modelled as 19.17 kg spherical masses of C4, and were detonated 1 m above ground in the centre of the domain. An array of pressure probes were placed at 1 m spacings in the same plane as the centre of the charge, providing 256 pairs of peak pressure and peak specific impulse per analysis.

The effects of obstacle density and positioning were tested. Nine cases were tested in total: four examining the influence of obstacle density (obstacles placed with uniform distribution and densities of 0.2, 0.5, 1.0 and 1.4 obstacles/m²); four examining the influence of obstacle bias (either ‘towards’ or ‘away’ from the charge, normally distributed with standard deviations of 2.29 m and 3.40 m); and a benchmark case of the blast occurring in an empty room. 20 simulations were run for each of the cases with obstacles present in order to build statistically robust datasets (5,120 pairs of pressure and impulse per case).

Compiling blast parameters against scaled distance allowed for the influence of channelling (values greater than the empty room case) and shielding (values less than the empty room case) to be readily observed, as a function of distance from the explosive. The results showed that channelling dominates closest to the charge, with specific impulse considerably more sensitive to enhancements from trapping and confinement than peak pressure. Specific impulse in regions closest to the charge was seen to increase with an increasing proportion of obstacles located near the charge; either through increasing obstacle density or through a bias towards the charge. For the highest density obstacle arrangement, peak specific impulse was around 2–3 times higher than the empty room values at $0.4 \text{ m/kg}^{1/3}$, whereas peak pressure was unaffected. As the distance from the charge increases, the effects of shielding become dominant, and the behaviour is reversed and specific impulse decreases as obstacle density increases. Peak pressure appears insensitive to channelling, but sensitive to shielding. For the highest density obstacle arrangement, peak pressure and peak specific impulse were around half the empty room values at $3.6 \text{ m/kg}^{1/3}$.

It is hypothesised that channelling is a localised effect, whereas shielding is cumulative. As the blast wave begins to interact with obstacles a number of preferential pathways are established. As the blast wave continues to propagate, it encounters more obstacles and the pathways begin to close. As distance from the blast increases, the likelihood that a preferential pathway will be obstructed increases, therefore channelling becomes less significant and shielding becomes dominant. The transition between channelling-dominant and shielding-dominant loading is a function of obstacle distribution: the more obstacles closer

to the charge, the quicker shielding becomes dominant. In order, the transition occurred at the smallest scaled distances for the ‘bias towards’ cases, the largest scaled distances for the ‘bias away’ cases, and intermediate scaled distance for the ‘no bias’ cases. The transition point was insensitive to obstacle density for the ‘no bias’ cases.

Overall, the presence of obstacles has a significant influence on the median pressure in the domain (reduces with increasing obstacle density), and a lesser influence on the variability of pressure in the domain (slightly increases with increasing obstacle density). Conversely, the presence of obstacles has a significant influence on the variability of impulse in the domain (increases with increasing obstacle density), and a lesser influence on the median pressure in the domain (slightly reduces with increasing obstacle density).

The research described in this article provides a suitable framework for the development of quick-running tools for predicting blast loading in a crowded internal environment. Numerical analysis has been used to populate a comprehensive suite of loading distributions to account for various arrangements and biases of obstacles within a domain. Simple observations relating to pressure/impulse percentiles and standard deviations, both for the entire domain and as a function of scaled distance, are used to compare each case against the results from a baseline model (e.g., an empty room). It is suggested that this framework is used in the future to derive methods to convert from one to the other, i.e., augmenting the results from a simple baseline model to better represent the magnitudes and variability of loading parameters in the complex case, without the associated computational expense. Further work could also expand on the initial framework by performing additional simulations to incorporate probabilistic variations in charge mass and type, domain size, confinement, and detonation location, as well as consideration of model error.

Declaration of competing interest

The authors declare that they have no known competing financial interests or personal relationships that could have appeared to influence the work reported in this paper.

References

- [1] M.D. Netherton, M.G. Stewart, Blast load variability and accuracy of blast load prediction models, *Int. J. Prot. Struct.* 1 (4) (2010) 543–570.
- [2] D. Cormie, G. Mays, P. Smith, *Blast Effects on Buildings*, Thomas Telford, London, 2012.
- [3] M. Larcher, F. Casadeia, Explosions in complex geometries – A comparison of several approaches, *Int. J. Prot. Struct.* 1 (2) (2010) 169–196.
- [4] M. Ben-Ezra, Y. Hamama-Raz, M. Mahat-Shamir, Psychological reactions to the 2017 Manchester Arena bombing: A population based study, *J. Psychiatr. Res.* 95 (2017) 235–237.

- [5] K. Hazel Kwon, Monica Chadha, Kirstin Pellizzaro, Proximity and terrorism news in social media: A construal-level theoretical approach to networked framing of terrorism in Twitter, *Mass Commun. Soc.* 20 (6) (2017) 869–894.
- [6] S.E. Rigby, T.J. Lodge, S. Alotaibi, A.D. Barr, S.D. Clarke, G.S. Langdon, A. Tyas, Preliminary yield estimation of the 2020 Beirut explosion using video footage from social media, *Shock Waves* 30 (6) (2020) 671–675.
- [7] G.C. Duncan-Miller, Urban Blast Waves: a Semi-Analytic Solution for Intense Explosions with Rigid Wall Reflections (Ph.D. thesis), Department of Mathematics, New Mexico Institute of Mining and Technology, Socorro, NM, USA, 2016.
- [8] G. Giannopoulos, M. Larcher, F. Casadei, G. Solomos, Risk assessment of the fatality due to explosion in land mass transport infrastructure by fast transient dynamic analysis, *J. Hazard. Mater.* 173 (2009) 401–408.
- [9] D. Alterman, M.G. Stewart, M.D. Netherton, Probabilistic assessment of airblast variability and fatality risk estimation for explosive blasts in confined building spaces, *Int. J. Prot. Struct.* 10 (3) (2019) 306–329.
- [10] A.A. Dennis, J.J. Pannell, D.J. Smyl, S.E. Rigby, Prediction of blast loading in an internal environment using artificial neural networks, *Int. J. Prot. Struct.* 12 (3) (2020) 287–314.
- [11] B. Willenborg, Simulation of Explosions in Urban Space and Result Analysis Based on Citygml-City Models and a Cloud-Based 3D-Webclient (Master's thesis), Technical University Munich, Munich, Germany, 2015.
- [12] W. Drazin, Blast Propagation and Damage in Urban Topographies (Ph.D. thesis), The Laboratory for Scientific Computing, Cavendish Laboratory, University of Cambridge, UK, 2017.
- [13] L. Mohr, R. Benauer, P. Leitl, F. Fraundorfer, Damage estimation of explosions in urban environments by simulation, in: *International Archives of the Photogrammetry, Remote Sensing and Spatial Information Sciences – ISPRS Archives Volume XLII-3/W8. Gidm 2019 – Geoinformation for Disaster Management*, Prague, Czech Republic, 42, 2019, pp. 253–260.
- [14] G. Valsamos, M. Larcher, F. Casadei, Beirut explosion 2020: A case study for a large-scale urban blast simulation, *Saf. Sci.* 137 (2021) 105190.
- [15] M. Silvestrini, B. Genova, F.J. Leon Trujillo, Energy concentration factor. A simple concept for the prediction of blast propagation in partially confined geometries, *J. Loss Prevent. Process Ind.* 22 (2009) 449–454.
- [16] K. Suzuki, H. Himeki, T. Watanuki, T. Abe, Experimental Studies on Characteristics of Shock Wave Propagation Through Cylinder Array, Technical Report, Japan Institute of Space and Astronautical Science, 2000.
- [17] S.S. Prasanna Kumar, S.V. Patnaik, K. Ramamurthi, Prediction of air blast mitigation in an array of rigid obstacles using smoothed particle hydrodynamics, *Phys. Fluids* 30 (2018) 046105.
- [18] A. Chaudhuri, A. Hadjadj, Sadot O., G. Ben-Dor, Numerical study of shock-wave mitigation through matrices of solid obstacles, *Shock Waves* 23 (2012) 91–101.
- [19] Q. Wan, V. Eliasson, Numerical study of shock wave attenuation in two-dimensional ducts using solid obstacles: How to utilize shock focusing techniques to attenuate shock waves, *Aerospace* 2 (2015) 203–221.
- [20] A. Hahn, M. Mensinger, M. Rutner, Peak overpressure and impulse due to diffraction over a cylinder and/or multi-reflection of a shockwave in structural design – part 1, *Int. J. Prot. Struct.* 12 (1) (2020) 22–48.
- [21] P.A. Shirbhate, M.D. Goel, A critical review of blast wave parameters and approaches for blast load mitigation, *Arch. Comput. Methods Eng.* 28 (2020) 1713–1730.
- [22] R. Hajek, M. Foglar, Numerical and experimental analysis of the effect of rigid barriers on blast wave propagation, *J. Struct. Eng.* 141 (12) (2015) 04015061.
- [23] A. Gautier, I. Sochet, E. Lapebie, A. Boubrir, Shock wave propagation in an obstructed area, *WIT Trans. Built Environ.* 198 (2020) 15–27.
- [24] W. Xiao, M. Andrae, N. Gebbeken, Experimental and numerical investigations of shock wave attenuation effects using protective barriers made of steel posts, *J. Struct. Eng.* 144 (11) (2018) 04018204.
- [25] W. Xiao, M. Andrae, N. Gebbeken, Numerical study on impulse reduction performance of protective barriers made of steel posts, *J. Struct. Eng.* 146 (10) (2020).
- [26] P.D. Smith, G.P. Whalen, L.J. Feng, T.A. Rose, Blast loading on buildings from explosions in city streets, *Struct. Build.* 46 (2000) 47–55.
- [27] P.D. Smith, T.A. Rose, Blast wave propagation in city streets – an overview, *Prog. Struct. Eng. Mater.* 8 (1) (2006) 16–28.
- [28] P.D. Smith, T.A. Rose, S.H. Ng, The influence of areal density on the shielding and channelling of blast by buildings, in: *18th International Symposium on Military Aspects of Blast and Shock*, Bad Reichenhall, Germany, 2004.
- [29] O. Pennetier, M. William-Louis, A. Langlet, Numerical and reduced-scale experimental investigation of blast wave shape in underground transportation infrastructure, *Process Saf. Environ. Prot.* 94 (2015) 96–104.
- [30] T. Anthistle, D.I. Fletcher, A. Tyas, Characterisation of blast loading in complex, confined geometries using quarter symmetry experimental methods, *Shock Waves* 26 (2016) 749–757.
- [31] G. Seisson, T. Lacaze, A. Rouquand, Uncertainty estimation of external blast effects using the Monte-Carlo method, in: *Structures Under Shock And Impact*, Vol. XVI, 2020, pp. 81–92.
- [32] Y. Shi, M.G. Stewart, Spatial reliability analysis of explosive blast load damage to reinforced concrete column, *Struct. Saf.* 53 (2014) 13–25.
- [33] M.D. Netherton, M.G. Stewart, The effects of explosive blast load variability on safety hazard and damage risks for monolithic window glazing, *Int. J. Impact Eng.* 36 (2009) 1346–1354.
- [34] Y. Ding, X. Song, H. Zhu, Probabilistic progressive collapse analysis of steel-concrete composite floor systems, *J. Constr. Steel Res.* 129 (2016) 129–140.
- [35] Y. Ding, X. Song, H. Zhu, Probabilistic progressive collapse analysis of steel frame structures against blast loads, *Eng. Struct.* 147 (2017) 679–691.
- [36] N.A. Marks, M.G. Stewart, M.D. Netherton, C.G. Stirling, Airblast variability and fatality risks from a VBIED in a complex urban environment, *Reliab. Eng. Syst. Saf.* 209 (2021) 107459.
- [37] J. Heylmun, P. Vonk, T. Brewer, BlastFoam 4.0 User Guide, Synthetik Applied Technologies, Austin, TX, USA, 2020.
- [38] C.N. Kingery, G. Bulmash, Airblast Parameters from TNT Spherical Air Burst and Hemispherical Surface Burst, Technical Report ARBRL-TR-02555, US Army BRL, Aberdeen Proving Ground, MD, USA, 1984.
- [39] T.R. Brewer, P.J. Vonk, J. Heylmun, Blastfoam: a free and open-source CFD airblast code for simulating high-explosive detonation, *Explos. Eng.* December 2020 (2020) 27–31.
- [40] T.R. Brewer, P.J. Vonk, J. Heylmun, Validation of the Blastfoam Airblast Solver, Technical Report 18–045, Synthetik Applied Technologies, Austin, TX, USA, 2020.
- [41] P.D. Lax, X.-D. Liu, Solution of two-dimensional Riemann problems of gas dynamics by positive schemes, *SIAM J. Sci. Comput.* 19 (2) (1998) 319–340.
- [42] P. Woodward, P. Colella, The numerical simulation of two-dimensional fluid flow with strong shocks, *J. Comput. Phys.* 54 (1) (1984) 115–173.
- [43] L.L. Sedov, *Similarity and Dimensional Methods in Mechanics*, New York Academic Press, NY, USA, 1959.
- [44] C.E. Joachim, G.W. McMahan, C.V. Lunderman, S.B. Garner, Airblast Effects Research: Small-Scale Experiments and Calculations, Technical Report SL-99-5, US Army Corps of Engineers, Waterways Experiment Station, Vicksburg, MS, USA, 1999.
- [45] M. Brittle, Blast Propagation in a Geometrically Complex Environment (Ph.D. thesis), Cranfield University, 2004.
- [46] S.E. Rigby, S.D. Fay, A. Tyas, J.A. Warren, S.D. Clarke, Angle of incidence effects on far-field positive and negative phase blast parameters, *Int. J. Prot. Struct.* 6 (1) (2015) 23–42.
- [47] A. Tyas, J.J. Reay, S.D. Fay, S.D. Clarke, S.E. Rigby, J.A. Warren, D.J. Pope, Experimental studies of the effect of rapid afterburn on shock development of near-field explosions, *Int. J. Prot. Struct.* 7 (3) (2016) 456–465.
- [48] <https://github.com/synthetik-technologies/blastfoam/tree/master/validation/blastfoam>. (Accessed 5 January 2022).
- [49] K.L. Gan, Characterising Effects of Human Scale Obstacles on Blast Loading in Confined Spaces, University of Sheffield, Sheffield, UK, 2021.
- [50] T. Payne, A. Williams, T. Worfolk, S. Rigby, Numerical investigation into the influence of cubicle positioning in large-scale explosive arena trials, *Int. J. Prot. Struct.* 7 (4) (2016) 547–560.
- [51] J.W. Denny, S.K. Clublely, Long-duration blast loading and response of steel column sections at different angles of incidence, *Eng. Struct.* 178 (2019) 331–342.
- [52] D. Bogosian, M. Yokota, S.E. Rigby, TNT Equivalence of C-4 and PE4: a review of traditional sources and recent data, in: *Proceedings of the 24th Military Aspects of Blast and Shock*, Halifax, Nova Scotia, Canada, 2016.
- [53] S.E. Rigby, P. Sielicki, An investigation of TNT equivalence of hemispherical PE4 charges, *Eng. Trans.* 62 (4) (2014) 423–435.
- [54] D. Rettenmaier, D. Deising, Y. Ouedraogo, E. Gjonaj, H. De Gersem, D. Bothe, C. Tropea, H. Marschall, Load balanced 2D and 3D adaptive mesh refinement in OpenFOAM, *SoftwareX* 10 (2019) 100317.
- [55] P.W. Sielicki, T. Gajewski, Numerical assessment of the human body response to a ground-level explosion, *Comput. Methods Biomech. Biomed. Eng.* 22 (2) (2018) 180–205.
- [56] D.J. Pope, The development of a quick-running prediction tool for the assessment of human injury owing to terrorist attack within crowded metropolitan environments, *Phil. Trans. R. Soc. B* 366 (1562) (2011) 127–143.
- [57] I. Kaleps, R.P. White, R.M. Beecher, J. Whitestone, L.A. Obergefell, Measurement of Hybrid III Dummy Properties and Analytical Simulation Database Development, Technical Report, Fort Belvoir: Defense Technical Information Center, 2020.
- [58] BBC, Statistics reveal Britain's 'Mr and Mrs average', 2010, <https://www.bbc.co.uk/news/uk-11534042>. (Accessed 29 September 2021).
- [59] W. Daamen, Modelling Passenger Flows in Public Transport Facilities (Ph.D. thesis), Delft University of Technology, 2004.
- [60] W.E. Baker, *Explosions in Air*, University of Texas Press, Austin, TX, USA, 1973.